Solar Phys (2008) 249: 85–101
DOI 10.1007/s11207-008-9161-4

Stream Interactions and Interplanetary Coronal Mass Ejections at 0.72 AU

L.K. Jian · C.T. Russell · J.G. Luhmann · R.M. Skoug · J.T. Steinberg

Received: 21 September 2007 / Accepted: 3 March 2008 / Published online: 28 March 2008

Abstract We present comprehensive surveys of 203 stream interaction regions (SIRs) and 124 interplanetary CMEs (ICMEs) during 1979 – 1988 using *Pioneer Venus Orbiter* (PVO) *in situ* solar-wind observations at 0.72 AU and examine the solar-cycle variations of the occurrence rate, shock association rate, duration, width, maximum total perpendicular pressure (P_t), maximum dynamic pressure, maximum magnetic field intensity, and maximum velocity change of these two large-scale solar-wind structures. The medians, averages, and histogram distributions of these parameters are also reported. Furthermore, we sort ICMEs into three groups based on the temporal profiles of P_t, and we investigate the variations of the fractional occurrence rate of three groups of ICMEs with solar activity. We find that the fractional occurrence rate of magnetic-cloud-like ICMEs declined with solar activity, consistent with our former 1-AU results. This study at 0.72 AU provides a point of comparison in the inner heliosphere for examining the radial evolution of SIRs and ICMEs. The width of

Electronic supplementary material The online version of this article (http://dx.doi.org/10.1007/s11207-008-9161-4) contains supplementary material, which is available to authorized users.

L.K. Jian (✉) · C.T. Russell
Institute of Geophysics and Planetary Physics, University of California, Los Angeles, 595 Charles E. Young Dr. East, 6862 Slichter, Los Angeles, CA 90095, USA
e-mail: jlan@igpp.ucla.edu

C.T. Russell
e-mail: ctrussel@igpp.ucla.edu

J.G. Luhmann
Space Sciences Laboratory, University of California, Berkeley, Berkeley, CA 94720, USA
e-mail: jgluhman@ssl.berkeley.edu

R.M. Skoug · J.T. Steinberg
Space Science and Applications, Los Alamos National Laboratory, Los Alamos, NM 87545, USA

R.M. Skoug
e-mail: rskoug@lanl.gov

J.T. Steinberg
e-mail: jsteinberg@lanl.gov

SIRs and ICMEs increases by 0.04 and 0.1 AU, respectively, and the maximum P_t decreases to about 1/3 from Venus to Earth orbit. In addition, our work establishes the statistical properties of the solar-wind conditions at 0.72 AU that control the solar-wind interaction with Venus and its atmosphere loss by related processes.

Keywords Stream interactions · Interplanetary coronal mass ejections · Venus · Solar wind · Inner heliosphere · Dynamic pressure · Flux rope · Shock · Solar cycle variation · Interplanetary magnetic field

1. Introduction

Two important types of large-spatial-scale solar-wind structures are stream interaction regions (SIRs) and interplanetary coronal mass ejections (ICMEs). The coronal source regions of the fast and slow streams, respectively coronal holes and streamer belts, are slowly varying; and the stream interactions they produce are quasi-stationary in a reference rotating with the Sun, lasting at times for many solar rotations. In contrast, the onset of the CME that leads to the more distant ICME may last only hours, and the ICMEs are transient features in the solar wind. The quasi-steady fast and slow streams and their resulting SIRs provide the background in the heliosphere for temporal solar disturbances (*e.g.*, the CMEs).

The fast streams can extend to low latitude after emerging from coronal holes at high or middle heliolatitude (*e.g.*, Krieger, Timothy, and Roelof, 1973), and sometimes they originate from coronal holes at low heliolatitude. As the Sun rotates, near the equatorial plane, a fast stream can overtake a preceding slow stream arising in the streamer belt (Feldman *et al.*, 1981; Gosling *et al.*, 1981), forming a SIR where the total pressure piles up, as illustrated in Figure 1. Behind the SIR, the fast stream outruns the trailing slow stream, forming a rarefaction region. Forward and reverse shock pairs may also form at the edges of the SIR. For a recent review see Balogh *et al.* (1999a).

Since coronal sources can change significantly on the time scale of one solar rotation (Balogh *et al.*, 1999b), some stream interactions are similarly transitory. SIRs that recur with a rough period of one solar rotation cycle are commonly called corotating interaction regions (CIRs) (Belcher and Davis, 1971; Smith and Wolfe, 1976; Gosling and Pizzo, 1999). Although we include CIRs in our SIR statistics, we separately study the properties of the long-lived CIRs.

ICMEs are the interplanetary counterpart of CMEs. They are commonly characterized by a stronger than ambient magnetic field, a rotating magnetic field, low β, low ion temperature, high α/proton density ratio, counterstreaming suprathermal electron strahl, declining velocity, and unusual ion charge states (*e.g.*, Gosling *et al.*, 1991; Neugebauer and Goldstein, 1997; Gosling and Forsyth, 2001; Cane and Richardson, 2003; Russell and Shinde, 2005; Wimmer-Schweingruber *et al.*, 2006; Zurbuchen and Richardson, 2006). Many ICMEs do not include all these signatures, and signatures are not always apparent. In addition, none of these features appears to be unique to ICMEs or by itself a sufficient condition to identify an ICME (*e.g.*, Gosling, 1997; Neugebauer and Goldstein, 1997; Wimmer-Schweingruber *et al.*, 2006), so the identification of ICMEs usually involves several signatures.

ICMEs frequently consist of several parts: a leading sheath-like pileup of solar-wind plasma and field, sometimes preceded by a forward shock, and a driver or ejecta portion that is thought to carry new magnetic field injected from the corona into the heliosphere by the CME. The ICMEs characterized by low β and coherent internal magnetic-field rotations through a relatively large angle (*e.g.*, Burlaga *et al.*, 1981; Klein and Burlaga, 1982;

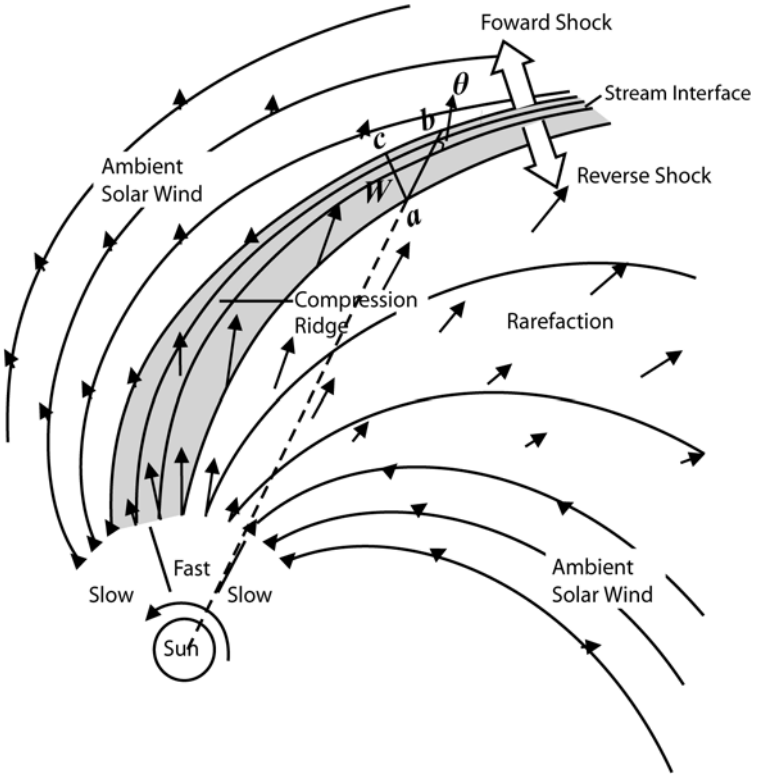

Figure 1 Schematic illustrating 2-D corotating stream structure in the solar equatorial plane in the inner heliosphere (after Pizzo, 1978). The SIR is in gray. The line ab indicates the radial extent of the SIR, which is the product of the duration and mean velocity. In 3-D geometry, there is a width of the SIR perpendicular to the stream interface. The line ac (W) is approximated as the projected length of such a width in the equatorial plane. W is approximately the product of radial extent ab and the sine of the spiral angle θ.

Lepping, Jones, and Burlaga, 1990) are called magnetic clouds (MCs) and are often treated as a specific subset of ICMEs.

Previous studies have suggested that flux ropes may exist prior to CME eruption (*e.g.*, Plunkett *et al.*, 2000; Rust *et al.*, 2005) or may be formed by reconnection during eruption. In any case, it is possible that ICMEs all contain a well-defined flux rope close to the Sun (Marubashi, 1997). As they evolve outward from the Sun, some flux-rope signatures may weaken (*e.g.*, Osherovich and Burlaga, 1997). In addition, some ICMEs may be encountered by the spacecraft far from the flux-rope axis where the flux-rope signatures are not clearly exhibited (*e.g.*, Jian *et al.*, 2005a, 2006b; Riley *et al.*, 2006).

ICMEs and SIRs are two major drivers of geomagnetic events. To fully understand the character of the inner heliosphere and to predict space weather, it is necessary to understand the radial evolution of SIRs and ICMEs in the inner heliosphere. Heliospheric models need such observations as inputs and empirical constraints. In a previous study, we carried out an extensive survey of SIRs and ICMEs at 1 AU (Jian *et al.*, 2006a, 2006b). Here we extend our systematic study of solar-wind structures to a heliospheric location inside 1 AU, enabling us to determine the statistical radial evolution of the properties of these two major drivers of geomagnetic activity.

Some information about the solar wind has been provided by studies from *Helios* (*e.g.*, Richter and Luttrell, 1986; Schwenn and Marsch, 1990). However, because of its very eccentric orbit from 0.3 to 1 AU, *Helios* did not provide long-term continuous observations at any fixed heliocentric distance except perhaps at 1 AU. In contrast, *Pioneer Venus Orbiter* (PVO) spent over 10 years in the solar wind at 0.72 AU, covering almost a full solar cycle at a fixed heliocentric distance, providing an ideal data set for such a study.

Another benefit of this study is that it provides characterization of the space environment near Venus. Solar activity may have played an important role in the evolution of the Venus atmosphere (and that of other weakly magnetized planets; see Russell, 1991; Luhmann, Kasprzak, and Russell, 2007, and references therein). Strong solar-wind dynamic pressures and large interplanetary magnetic fields (IMFs) can cause compression and/or magnetization of the ionosphere of weakly magnetized Venus. Hence, a quantitative description of the strength of solar-wind structures at 0.72 AU is also an important component of such studies.

We first introduce the PVO solar-wind data set in Section 2, and then review our identification criteria and surveys of SIRs and ICMEs in Section 3. In Section 4, the solar-cycle variations and statistical distributions of the properties of SIRs and ICMEs are compared and discussed. In Section 5, we summarize our findings and compare them with measurements at 1 AU to understand the radial evolution better.

2. PVO Solar-Wind Data Set

The surveys of SIRs and ICMEs at 0.72 AU are based on solar-wind observations by PVO (Colin and Hunten, 1977; Colin, 1980) during January 1979 to August 1988. The plasma analyzer (Intriligator, Wolfe, and Mihalov, 1980) and magnetometer (Russell *et al.*, 1980) provided the solar-wind plasma and IMF measurements, respectively.

PVO orbited Venus in a highly elliptical trajectory with its line of apsides (joining periapsis and apoapsis) close to the ecliptic plane. When periapsis was in the Venus tail, the PVO spent most of the orbit in the solar wind except a few hours per day. About half a Venus year later, apoapsis was in the tail and for a couple of months PVO spent its entire orbit out of the undisturbed solar wind. Overall, the solar-wind data set covers 60.3% of the 10-year period. The annual usable data fraction varies from a maximum of 68% in 1982 to a minimum of 36% in 1988. Considering the data gaps, we used the observed event number divided by the fraction of usable data each terrestrial year to estimate the annual number of events for each year.

For our study, we used averaged 10-min resolution plasma data and 0.5-sec resolution magnetometer data. The temporal resolution of the magnetometer data is sufficient to identify shocks, even though the low temporal resolution plasma data by themselves would have provided somewhat ambiguous identifications. In combination, they allow us to identify interplanetary shocks, SIRs, and ICMEs and also quantify their characteristics, similar to our 1-AU study in Jian *et al.* (2006a, 2006b).

3. Criteria and Surveys

We used the total perpendicular pressure (P_t) as a key parameter to study SIRs and ICMEs (*e.g.*, Jian *et al.*, 2005a, 2005b). P_t is the sum of the magnetic pressure and plasma thermal pressure perpendicular to the magnetic field, that is, $B^2/(2\mu_0) + \sum_j n_j k T_{\mathrm{perp},j}$, where j represents the three major species in the solar-wind plasma: protons, electrons, and α particles.

P_t is a key parameter in determining the evolution of magnetic structures in the solar wind (Russell, Shinde, and Jian, 2005).

Owing to limitations of the PVO measurements, we had to make some assumptions. From the work of Pilipp *et al.* (1990) on solar-wind electron parameters between 0.3 and 1 AU, we took 200 000 K as the best estimate of the electron perpendicular temperature at 0.72 AU. Additionally, we assumed that 4% of ions are α particles (*e.g.*, Aellig, Lazarus, and Steinberg, 2001), the temperature of α particles is four times that of protons, and the ion temperatures are isotropic, consistent with the assumptions in our 1-AU study (Jian *et al.*, 2006a, 2006b).

SIRs were identified by inspection of data based on several features: an increase of solar-wind speed V_p, a peak of P_t with gradual decreases at both sides, an increase of proton number density N_p, a compression of magnetic field $\boldsymbol{B}$, an enhancement of proton temperature T_p, and an increase of the entropy [defined as $\ln(T_p^{3/2}/N_p)$] (Intriligator and Siscoe, 1994; Neugebauer *et al.*, 2004). Velocity vector components were unavailable, so we were unable to look for characteristic flow deflections. Figure 1(1) of Jian *et al.* (2008) shows a classical SIR observed by PVO. The P_t gradient arises to retard and deflect the plasma that flows toward the interface from both sides in the stream interface (SI) fixed reference frame. In other words, the dynamic pressure P_{dyn} of the flow on both sides of the interface expressed in the SI reference frame is balanced by the P_t centered on the interface. The time of the SI passage (*e.g.*, Burlaga, 1974; Gosling *et al.*, 1978; Schwenn, 1990) was identified as the time at which P_t maximized within an interval of increasing V_p. In many events, the identification of the SI was also verified by the compression of N_p and $\boldsymbol{B}$ as the SI was approached from either side, and by the enhancement of T_p.

We identified ICMEs by inspection based on a combination of ICME signatures: a P_t enhancement, a stronger than ambient $\boldsymbol{B}$, a relatively quiet and smooth rotation in $\boldsymbol{B}$, a low T_p, and a declining V_p (Jian *et al.*, 2006b; see Figure 2(1) of Jian *et al.* (2008) for an example). The α abundance and electron flux data were unavailable from the PVO data set. At least three of these features were required to identify an ICME. The edges of ICMEs were determined from a consensus of the available features listed here, usually also delimited by sharp changes in plasma parameters and magnetic field (Wimmer-Schweingruber *et al.*, 2006).

In our study of ICMEs at 1 AU, we found that the P_t temporal profiles of ICMEs could be roughly sorted into three characteristic patterns, which were associated with the observed MC signatures (Jian *et al.*, 2005a, 2006b). Corresponding to the Group 1, 2, and 3 ICMEs, the P_t profile following the shock and/or sheath enhancements (often existing but not always) has, respectively, a central pressure maximum, a steady plateau, or a gradual decay. This pattern is consistent with a model in which each ICME has a central flux rope, and the three groups of P_t profiles are due to different distances to the central flux rope at closest approach. Magnetic clouds, where the spacecraft observes a clear flux rope, most often are classified as Group 1 ICMEs. Of our Group 1 events at 1 AU, 89% are in the MC list of Cane and Richardson (2003), and 62% are in Lepping's MC table (Jian *et al.*, 2006b). In contrast, Group 3 ICMEs rarely show a flux-rope geometry, consistent with an encounter in which flux-rope intersection is grazing or missing (Jian *et al.*, 2006b).

A few of the SIRs and ICMEs have irregular P_t profiles, usually caused by mutual interactions, which may produce complex structures (*e.g.*, Burlaga *et al.*, 1981) or complicated solar imprint. If the structures are still representative, we included them in the SIR or ICME list. The ICMEs with irregular P_t profiles were not assigned to any group. In addition, data gaps prevented us from assigning a category for some ICMEs.

In Appendices I and II, we report comprehensive surveys of SIRs and ICMEs observed by PVO during 1979 to 1988, encompassing the maximum and declining phase of solar cycle 21 and the rising phase of solar cycle 22. CIRs and hybrid events consisting of more than one event (*e.g.*, Crooker, 2000) have been marked in the surveys. The start and end time, associated shocks, maximum of $P_{\rm t}$ ($P_{\rm tmax}$), maximum of $P_{\rm dyn}$ ($P_{\rm dynmax}$), maximum field intensity ($B_{\rm max}$), $V_{\rm max}$ and $V_{\rm min}$ within each event (including the start and end points), and the group classification of ICMEs are all tabulated. For SIRs, the $V_{\rm max}$ and $V_{\rm min}$ are the maximum and minimum speeds within the interaction region.

In addition, we measured the maximum velocity change with time over one event (ΔV). Since the velocity increases over a SIR, the ΔV is $V_{\rm max} - V_{\rm min}$, indicating the velocity variation from slow to fast stream within the interaction region including the very start and end points. However, most ICMEs (92%) in our survey have a negative ΔV (*i.e.*, decreasing velocity with time). Besides the possible effects of solar imprint, such velocity-declining behavior suggests that most ICMEs are expanding at 0.72 AU. In the following, we only consider the absolute maximum velocity change ($|\Delta V|$) for ICMEs, which is also defined as the expansion speed of ICMEs (*e.g.*, Jian *et al.* (2008) and references therein). In any case, $|\Delta V|$ for both SIRs and ICMEs is $V_{\rm max} - V_{\rm min}$.

4. Properties of SIRs and ICMEs

In this section we discuss the results of our survey of the properties of SIRs and ICMEs, as presented in Tables 1 and 2 and Figures 2–4. Tables 1 and 2, respectively, list the annual averages as well as the statistics of the properties of the 203 SIRs and 124 ICMEs at 0.72 AU from 1979 to 1988. Owing to different fractions of data gaps in each year, we normalized the annual number of events by the fraction of available data during each terrestrial year and listed them in parentheses in the two tables. The average, median, maximum, and minimum values of each parameter are given in the bottom four lines.

In Figure 2a, the annual mean of sunspot number (SSN) indicates the solar activity level. The other panels of Figure 2 compare the solar-cycle variations of the following properties of SIRs and ICMEs: number of observed events (and the normalized number of events if data are available for a full year, marked by diamonds), duration, width, $P_{\rm tmax}$, $P_{\rm dynmax}$, $B_{\rm max}$, and $|\Delta V|$. The bars indicate the corresponding probable errors of the mean. The y-axis scales for each parameter are the same for SIRs and ICMEs. The exact values are listed in Table 1 and 2. To characterize the properties of the solar-wind environment around Venus, histograms of these properties are also displayed in Figure 3. In the following subsections, we extensively describe and discuss each property, in turn: the occurrence rate, the shock association rate, the temporal and spatial scales, the maximum of the total perpendicular pressure, the maxima of the dynamical pressure and magnetic field intensity, and the absolute value of the maximum velocity change. Since the properties of CIRs mimic those of SIRs at 0.72 AU (Jian *et al.*, 2008), their solar-cycle variations and statistics are not given separately here.

4.1. Occurrence Rate of Events and Associated Shocks

As is evident from an examination of the data in Table 1, about half of SIRs recurred on two or more solar rotations. The fraction of CIRs among SIRs did not show a clear solar-cycle dependence. Long-term data gaps each year may affect our CIR counting. By considering the data gaps, the normalized annual number of SIRs ranged from 25 to 42, whereas the

Table 1 Statistics of SIRs at 0.72 AU.

Year	Observed (normalized)[a] No. of SIRs	Observed (normalized) No. of CIRs	% of CIRs among SIRs	⟨Width⟩ (AU)	$\langle P_{\mathrm{dynmax}} \rangle$ (nPa)	$\langle P_{\mathrm{tmax}} \rangle$ (pPa)	$\langle B_{\mathrm{max}} \rangle$ (nT)	$\langle \Delta V \rangle$ (km s^{-1})
1979	22 (32)	9 (13)	40.9	0.24 ± 0.03[b]	13.1 ± 1.0	365 ± 24	21.8 ± 1.2	210 ± 22
1980	23 (35)	13 (20)	56.5	0.28 ± 0.02	15.1 ± 1.6	364 ± 26	19.9 ± 1.1	222 ± 18
1981	16 (25)	8 (12)	50.0	0.24 ± 0.04	17.4 ± 1.7	565 ± 46	24.4 ± 2.1	203 ± 20
1982	20 (29)	10 (15)	50.0	0.24 ± 0.03	16.7 ± 1.5	561 ± 53	24.0 ± 1.4	266 ± 22
1983	25 (39)	14 (22)	56.0	0.24 ± 0.02	20.3 ± 2.4	525 ± 43	22.8 ± 1.1	264 ± 16
1984	20 (35)	9 (16)	45.0	0.23 ± 0.02	18.9 ± 1.3	567 ± 41	23.6 ± 1.0	280 ± 19
1985	18 (28)	9 (14)	50.0	0.13 ± 0.02	19.5 ± 1.2	502 ± 40	23.5 ± 1.5	216 ± 24
1986	19 (39)	6 (12)	31.6	0.17 ± 0.02	16.4 ± 1.6	360 ± 33	18.0 ± 1.1	163 ± 12
1987	25 (39)	15 (23)	60.0	0.17 ± 0.02	14.9 ± 0.9	356 ± 17	19.1 ± 0.8	197 ± 17
1988	15 (42)	6 (17)	40.0	0.19 ± 0.02	18.6 ± 3.1	483 ± 82	21.7 ± 2.2	201 ± 21
Average[c]	20 (34)	10 (16)	48.8	0.22 ± 0.01	17.0 ± 0.6	458 ± 14	21.8 ± 0.4	224 ± 6
Median[d]	20 (35)	9 (16)	50.0	0.20	15.5	410	20.5	215
Max[d]	25 (42)	15 (23)	60.0	0.75	61.0	1550	50.0	450
Min[d]	15 (25)	6 (12)	31.6	0.04	4.5	180	11.0	57

[a]The normalized number of events is in parentheses, considering the amount of available data during a terrestrial year.

[b]Average value ± the probable error of the mean.

[c]The averages of the first two parameters are the average annual numbers of observed (normalized) events; the average CIR fraction is the percentage of CIRs over all SIRs for the 10 years; the remaining five parameters are of all the events during the 10 years.

[d]The median/maximum/minimum values of the first three parameters are of the annual values; the median/maximum/minimum values for the last five parameters are of all the events during the 10 years.

Table 2 Statistics of ICMEs at 0.72 AU.

Year	Observed (normalized) No. of ICME	No. of ICMEs with shock	% of ICMEs with shock	⟨Width⟩ (AU)	$\langle P_{\rm dynmax}\rangle$ (nPa)	$\langle P_{\rm tmax}\rangle$ (pPa)	$\langle B_{\rm max}\rangle$ (nT)	$\langle \mid \Delta V \mid \rangle$ (km s^{-1})
1979	17 (25)	12	70.6	0.32 ± 0.05	22.8 ± 2.7	628 ± 98	31.1±3.4	141 ± 24
1980	20 (31)	10	50.0	0.26 ± 0.03	17.0 ± 2.3	435 ± 76	24.2±2.6	113 ± 14
1981	15 (23)	7	46.7	0.31 ± 0.06	32.2 ± 5.4	789 ± 148	34.6±5.1	177 ± 30
1982	21 (31)	16	76.2	0.30 ± 0.03	36.0 ± 4.4	1098 ± 163	40.4±4.1	141 ± 17
1983	10 (16)	4	40.0	0.27 ± 0.03	30.3 ± 6.6	785 ± 191	31.5±4.4	162 ± 24
1984	8 (14)	3	37.5	0.27 ± 0.06	35.3 ± 5.3	978 ± 165	40.1±5.3	128 ± 28
1985	7 (11)	2	28.6	0.29 ± 0.04	23.5 ± 2.2	482 ± 68	24.2±2.6	107 ± 17
1986	5 (10)	0	0.0	0.20 ± 0.06	18.9 ± 2.7	366 ± 65	19.1±2.4	80 ± 12
1987	12 (18)	3	25.0	0.26 ± 0.04	24.4 ± 3.6	680 ± 114	30.8±3.1	119 ± 21
1988	9 (25)	3	33.3	0.27 ± 0.04	14.3 ± 1.7	441 ± 51	22.8±2.2	95 ± 12
Average	12 (20)	6	47.6	0.28 ± 0.01	26.1 ± 1.5	704 ± 48	31.1 ± 1.4	132 ± 7
Median	11 (21)	4	38.8	0.27	20.7	560	26.0	115
Max	21 (31)	16	76.2	0.91	82.0	2500	77.0	410
Min	5 (10)	0	0.0	0.06	4.2	100	11.0	5

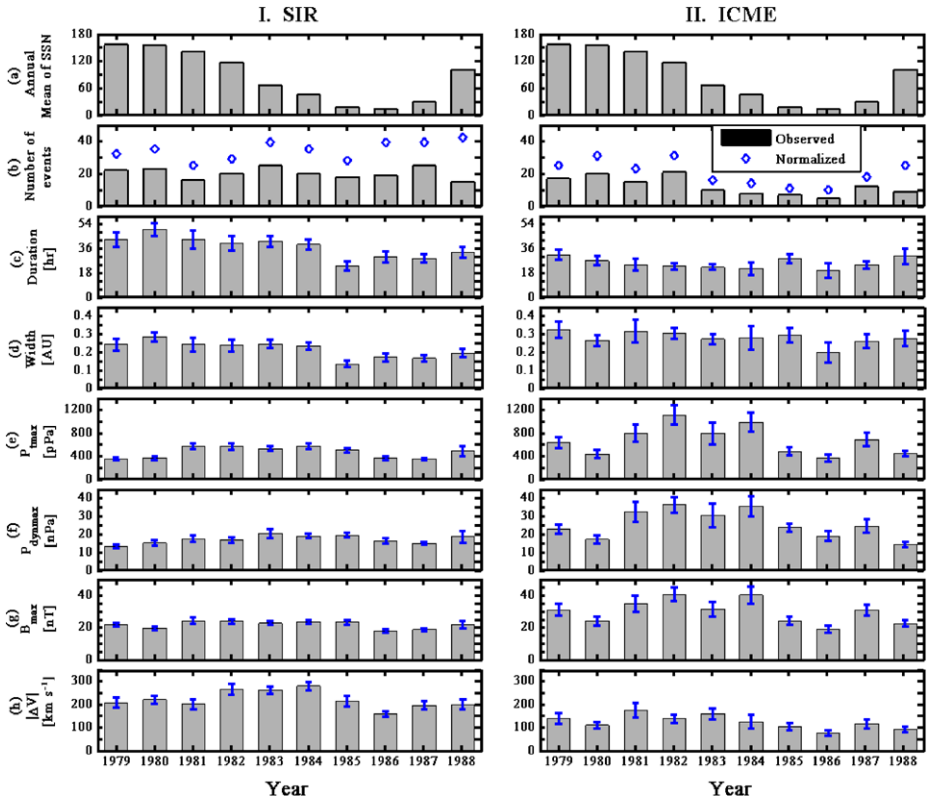

Figure 2 Solar-cycle variations of the properties of SIRs and ICMEs: (a) annual mean of sunspot number (SSN), (b) number of events (normalized number of events obtained by considering data gaps, marked by diamonds), (c) duration, (d) width (estimated by the product of duration and mean velocity, obtained by considering the Parker spiral angle for SIRs), (e) maximum of P_t, (f) maximum of P_{dyn}, (g) peak magnetic field intensity B_{max}, and (h) absolute of maximum velocity change within one event, $|\Delta V|$ ($V_{max} - V_{min}$). The scales for SIRs and ICMEs are the same for the same property.

number of CIRs ranged from 12 to 23. Neither the occurrence rate of SIRs nor that of CIRs showed a strong solar-cycle dependence, illustrated in Figure 2b, in contrast to the results of Lindsay *et al.* (1994), who found an inverse correlation between the occurrence of stream interactions and solar activity also based on the PVO data set. We believe the difference is due to our improved identification of SIRs using P_t as a primary criterion. The simple signature of the gradual pileup of P_t at the stream interface can readily reveal the compression produced by stream interaction, whereas the complicated temporal variations of individual plasma and magnetic field parameters are much more difficult to interpret. The prevalence of SIRs at all phases of the solar cycle is not very surprising, as velocity differentials at the coronal sources remain a feature of the solar wind at all times.

As shown in Table 2 and Figure 2, the normalized annual number of ICMEs varied nearly in phase with the solar cycle, from 10 to 31. This observation is in agreement with the 0.72-AU results of Lindsay *et al.* (1994) as well as Mulligan, Russell, and Luhmann (1998), although they used slightly different selection criteria. The solar-cycle dependence of the ICME occurrence rate roughly follows the solar-cycle dependence of the CME occurrence rate (*e.g.*, Gopalswamy, 2006; Riley *et al.*, 2006).

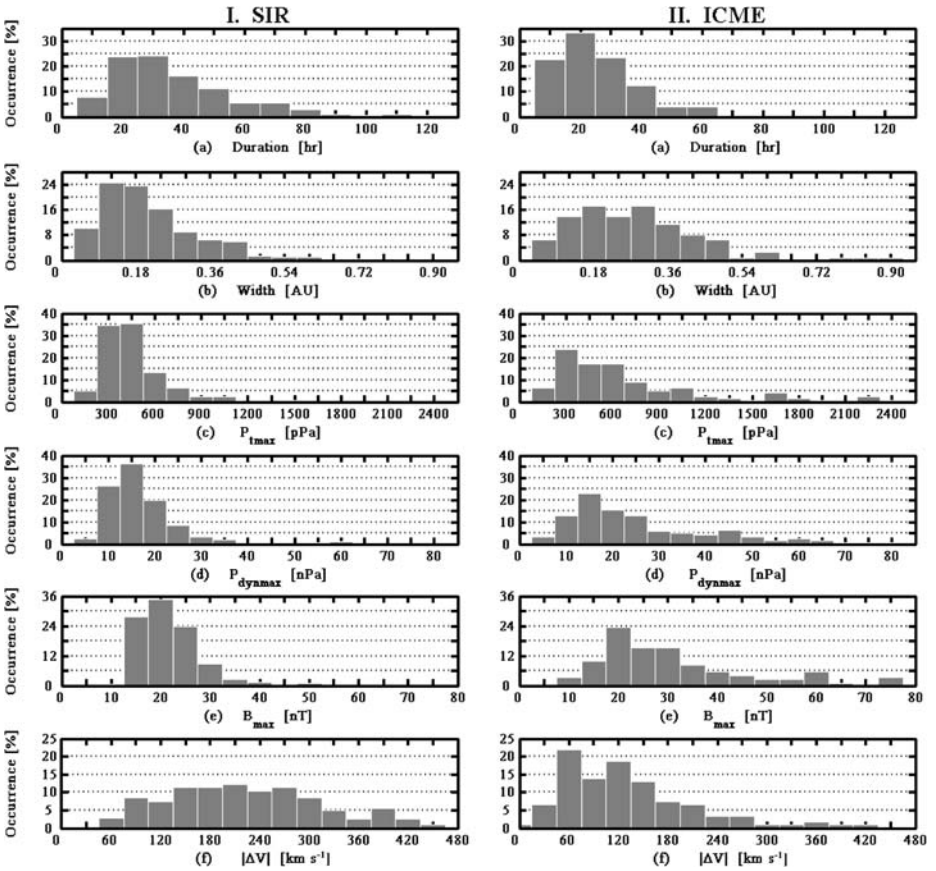

Figure 3 The histogram distributions of the properties of SIRs and ICMEs during 1979 – 1988: (a) duration, (b) width, (c) maximum of P_t, (d) maximum of P_{dyn}, (e) peak magnetic field intensity B_{max}, and (f) absolute of maximum velocity change $|\Delta V|$. The same parameters of SIRs and ICMEs are compared on the same scale.

Over the 10 years, 3% of SIRs occurred with shocks (data not shown), and 48% of ICMEs drove shocks (see Table 2). Most of the shocks associated with ICMEs were forward shocks. There was only one reverse shock associated with an ICME, and it occurred at the rear of the ICME, probably caused by the overtaking of a following fast stream. From Table 2, we can see that the annual shock association rate of ICMEs roughly varies in phase with solar activity, ranging from 0% to 76%.

4.2. Duration and Width

Our statistics show that SIRs typically lasted longer than ICMEs at 0.72 AU. The median duration of SIRs was 32.5 hours, whereas the median duration of ICMEs was 23.2 hours, demonstrated by Figure 3a. The duration of SIRs was also more variable than that of ICMEs, ranging from 7 hours to 122 hours. As shown in Figure 2c, the SIR durations were generally shorter around solar minimum (during 1985 – 1988) than in other years, whereas the ICME durations had no strong solar-cycle dependence.

From the product of duration and mean velocity (approximated by the mean of $V_{\max}$ and $V_{\min}$), we can roughly get the radial extent of one event. This product is useful to describe ICMEs, because the ICMEs propagate almost radially, if one considers the Parker spiral angle to be relatively small at 0.72 AU and given the short propagation time of ICMEs to 0.72 AU. However, the width perpendicular to the stream interface is more meaningful for the study of SIR evolution. To calculate such a width, we would need to get the normal direction of every interface and also to consider the 3-D geometry for each SIR. For a rough estimate, we projected the width into the solar equatorial plane, as line $ac(W)$ in Figure 1. We consider the spiral angle θ, which is $\arctan(r\omega/V_{\mathrm{r}})$, where r, ω, and V_{r} are, respectively, the heliocentric distance, solar rotation angular velocity, and radial component of solar-wind velocity. As illustrated in Figure 1, the projected width (W) of the SIR is approximately the product of duration, mean velocity, and $\sin\theta$. To be consistent in our terminology, we use one term, "width," for both SIRs and ICMEs, though it means projected width for SIRs and radial width for ICMEs.

Overall, at 0.72 AU, the median width was 0.20 AU for SIRs and 0.27 AU for ICMEs. For both SIRs and ICMEs, the solar-cycle variations of width mimicked duration, suggesting that the mean velocity did not play a critical role in determining the solar-cycle variation trend of width.

From the solar-cycle variations of SIR duration and width, we find that they were smaller around solar minimum. The widths of SIRs were less variable than ICMEs (see Figure 3b). There may be several factors causing the smaller duration and width near solar minimum. First, the peak fast-stream speed is lower at solar minimum, so there would be less compression. Second, around solar minimum, the heliospheric current sheet (HCS) is almost in the solar equatorial plane, just with slight wiggles (*e.g.*, Mariani and Neubauer, 1990; Suess and Hildner, 1985). The transition between slow and fast streams near the equatorial plane is not sharp. As the Sun rotates, the compression between the two streams could be weaker than other periods when the HCS is more tilted with respect to the equatorial plane.

In a general sense, the solar-cycle variations of the SIR width may also have something to do with the SIR-geometry variations over the solar cycle. Since the inclination of the HCS can vary significantly during a solar cycle, the change of our measured width in the equatorial plane does not necessarily proportionally represent the variation of the actual thickness perpendicular to the SI in three dimensions.

Among 124 ICMEs, 65 events had a sheath region leading the magnetic obstacle. The plasma was usually compressed greatly within the sheath region, so the sheath region can be highly geoeffective (Crooker, 2000; Huttunen *et al.*, 2005) and also effective in cosmic-ray Forbush decreases (*e.g.*, Burlaga, 1991). To be consistent for all ICMEs, the width of ICMEs in our study included the sheath region if there was one. Such a definition is meaningful in its own right because the sheath region has been commonly assumed as the interplanetary counterpart of the bright front (Forsyth *et al.*, 2006), which itself is one part of a three-part CME structure (Hundhausen, 1988). On average, the sheath region took about 16% of the duration and the width of ICMEs. Taking that into account, one sees that our result is consistent with the radial width of ICMEs and MCs at 0.72 AU in Bothmer and Schwenn (1994) as well as Wang, Du, and Richardson (2005), which both excluded the sheath region.

4.3. Maximum of Total Perpendicular Pressure

If one takes the median value, SIRs had a P_{tmax} of 410 pPa, whereas ICMEs had a P_{tmax} of 560 pPa at 0.72 AU, indicating a stronger pressure pileup could form because of the interaction associated with an ICME than because of the interaction between fast and slow

streams. In contrast, at 1 AU, the medians of $P_{\rm tmax}$ of SIRs and ICMEs become almost the same, about 150 pPa (Jian *et al.*, 2008). As shown in Figure 2e, $P_{\rm tmax}$ was larger during the declining phase, both for SIRs and ICMEs, although to different extents. Such solar-cycle dependence is similar to our 1-AU results (Jian *et al.*, 2006a, 2006b). The slightly larger $P_{\rm tmax}$ of SIRs during the declining phase is probably due to more faster streams over the that interval. The $P_{\rm tmax}$ of ICMEs in the declining phase was quite variable, so its average values had large error bars, but the averages can be twice that typically observed in other phases. The high $P_{\rm tmax}$ of ICMEs during 1981 – 1984 was probably caused by some fast CMEs appearing as the solar magnetic field reorganized itself from solar maximum to solar minimum (*e.g.*, see Figure 5 of Richardson, Cliver, and Cane, 2000).

As illustrated in Figure 3c, about 70% of the $P_{\rm tmax}$ of SIRs fell in a narrow range of 225 – 525 pPa, whereas 70% of the $P_{\rm tmax}$ of ICMEs were in a wider range of 225 – 975 pPa. This suggests that the interaction associated with an ICME is much more variable than the interaction between streams. In 62% of ICMEs containing a sheath region, $P_{\rm t}$ did not maximize in the sheath region but rather in the ICME core, suggesting that the magnetic obstacle born from the corona still holds a larger pressure despite strong compression and disturbances in the sheath region. We found that such ICMEs were classified in either our Group 1 or Group 2 ICMEs, if they had classifiable $P_{\rm t}$ patterns.

4.4. Maxima of Dynamic Pressure and Magnetic Field Intensity

Many studies have described the interaction between the solar wind and Venus (*e.g.*, Russell and Vaisberg, 1983; Vaisberg and Zeleny, 1984; Luhmann, 1986). In particular, the high $P_{\rm dyn}$ interaction can cause a reduction of the Venus ionopause altitude and the magnetization of the ionosphere (*e.g.*, Luhmann and Cravens, 1991). Both of these two results have the potential to increase pickup ion production and losses (Luhmann, Kasprzak, and Russell, 2007). For instance, PVO Neutral Mass Spectrometer (NMS) ion observations show that the escape fluxes were significantly enhanced during ICME and SIR passages (Luhmann, Kasprzak, and Russell, 2007). In addition, a large and relatively steady IMF can produce a magnetized ionosphere because the physics of the ionospheric magnetization process depends on the high field strength at its boundary, regardless of a field produced by the magnetosheath field compression or an intrinsically IMF (Luhmann, Kasprzak, and Russell, 2007). Therefore, in this section we specially describe maxima of $P_{\rm dyn}$ and B.

At Venus orbit, the $P_{\rm dyn}$ of general solar wind, regardless of any structures, is about 5 nPa. In contrast, the $P_{\rm dynmax}$ of SIRs had a median of 15.5 nPa, about three times of general solar wind. The $P_{\rm dynmax}$ of ICMEs was even larger, with a median of 20.7 nPa. The $P_{\rm dynmax}$ of ICMEs also had a greater variability, as shown in Figure 3d, with a long tail extending up to 82 nPa, indicating that ICMEs could play a critical role in compressing and magnetizing the ionosphere of Venus at times.

In about 81% of SIRs at 0.72 AU, $P_{\rm dyn}$ reached a peak within a 6-hour interval range from the stream interface. The $P_{\rm dynmax}$ appeared nearly equally in the sheath or driver of ICMEs. Over the 10-year period, stronger $P_{\rm dynmax}$ of ICMEs appeared in the declining phase of solar cycle 21, displayed in Figure 2f, consistent with the larger $P_{\rm dyn}$ of the solar wind during the same period from *Helios* measurements (Schwenn, 1990), and it was probably due to a greater number of very fast CMEs at that time (Sheeley *et al.*, 1985).

The median $B_{\rm max}$ values were 20.5 nT for SIRs and 26 nT for ICMEs. If we take 16 nT as the approximate average B of ICMEs, based on the radial dependence of ICME average B in Forsyth *et al.* (2006), we can get the compression rate of the magnetic field within an ICME of about a factor of 1.6. The solar-cycle variation of $B_{\rm max}$ mimicked $P_{\rm tmax}$, both

for SIRs and ICMEs, shown in Figures 2g and 2e, and was slightly higher in the declining phase. $B_{\max}$ was more variable for ICMEs than for SIRs (Figure 3e), similar to P_{tmax} again. Both the solar-cycle variation and histogram distribution suggest an important role for the magnetic field in P_{t}.

Overall, the solar-cycle variations of P_{dynmax} and $B_{\max}$ suggest that the declining phase may be a more interesting time period than other solar-cycle phases for studies of the solar-wind interaction with Venus. With larger median values and larger distribution variabilities of P_{dynmax} and $B_{\max}$, ICMEs could be very important to the interaction between the solar wind and Venus and to the loss and evolution of the Venus atmosphere.

4.5. Absolute Value of the Maximum Velocity Change

Introduced in Section 3, $|\Delta V|$ denotes the absolute value of the maximum velocity change within one event. It is also the expansion speed for ICMEs. As displayed in Figure 2h, the $|\Delta V|$ of SIRs was large during 1982 – 1984 (*i.e.*, the declining phase of solar cycle 21), whereas $|\Delta V|$ of ICMEs showed little solar-cycle dependence.

As illustrated Figure 3f, $|\Delta V|$ values of both SIRs and ICMEs were highly variable, in particular for SIRs. The median $|\Delta V|$ over a SIR was 215 km s^{-1}, being 100 km s^{-1} larger than the ICME median $|\Delta V|$, indicating a much larger velocity change associated with SIRs. Our $|\Delta V|$ of ICMEs (115 km s^{-1}) is compatible with the speed difference (80 – 120 km s^{-1}) inside the ICME leading and trailing edges from *Helios* observations (Forsyth *et al.*, 2006), although they defined the ICME expansion speed as half of $|\Delta V|$. Quantitatively, our $|\Delta V|$ is close to the Alfvén speed in the ICME as given by Forsyth *et al.* (2006), consistent with the conclusion in Wang, Du, and Richardson (2005).

5. Summary and Discussion

From Figure 2, the occurrence rate, P_{tmax}, P_{dynmax}, and $B_{\max}$ of ICMEs had relatively stronger solar-cycle dependence than those of SIRs; however, the duration, width, and $|\Delta V|$ of SIRs had clearer solar-cycle dependence than those of ICMEs. The average width, P_{tmax}, P_{dynmax}, and $B_{\max}$ of ICMEs were larger than for SIRs, whereas the average duration and $|\Delta V|$ of SIRs were larger than for ICMEs.

Interestingly, P_{tmax}, P_{dynmax}, $B_{\max}$, and $|\Delta V|$ of both ICMEs and SIRs were larger during the declining phase of solar cycle 21 than in other years, although to different extents. These enhancements are likely the result of the occasional strong solar activity that sometimes occurs in the declining phase (*e.g.*, Sheeley *et al.*, 1985), while high-speed streams occur as their coronal source regions at the poles are tilted or extended to lower heliolatitudes (*e.g.*, see Luhmann *et al.*, 2002, and references therein for a discussion of the solar-cycle variation of solar-wind sources). The strong solar activity during this period is also demonstrated by intense intervals of solar magnetic flux, which is sometimes even larger than the flux at SSN maximum (see Figure 1 in Song and Wang, 2006).

We were able to sort 78% of the ICMEs into three groups depending on the temporal profiles of P_{t}. In all, we observed 33 Group 1 and 25 Group 2 ICMEs during the 10 years. This is comparable with the amount of 61 MCs observed by Mulligan, Russell, and Luhmann (1998). Respectively, Group 1, 2, and 3 ICMEs were observed 27%, 20%, and 31% of the time. Figure 4 illustrates the solar-cycle variations of the fractional occurrence rates of the three groups of ICMEs and unclassifiable ICMEs at 0.72 and 1 AU. The variation trends are similar at the two locations. The extent of the vertical axis is the sum of the four fractions,

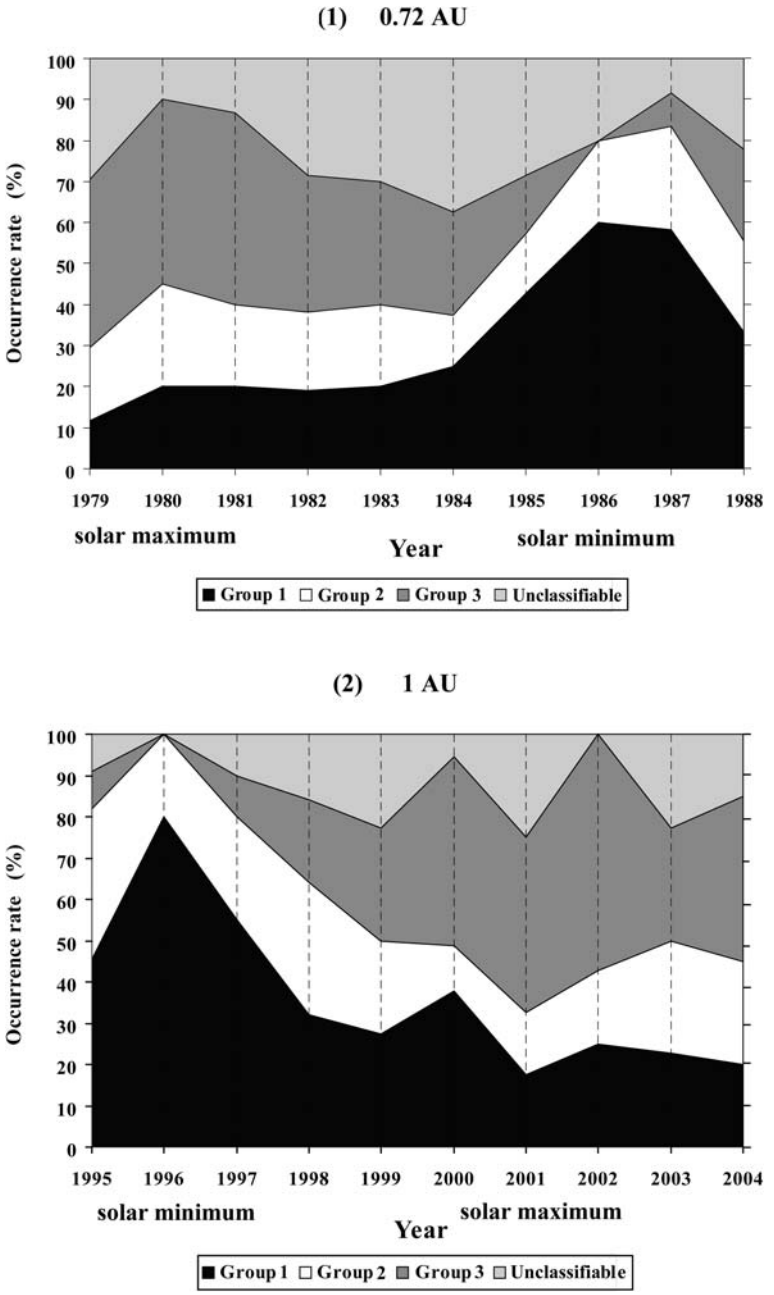

Figure 4 Fractional occurrence rates of Groups 1 to 3 and unclassifiable ICMEs at 0.72 AU and 1 AU.

which is 100% for each year. The fractional occurrence rate of Group 1 ICMEs (MC-like ICMEs; black region in Figure 4) varied inversely with solar activity, with a peak at solar minimum (1986 and 1996), in contrast to the variation of Group 3 ICMEs (dark gray). The

fractional occurrence rate of unclassifiable ICMEs did not show any clear solar-cycle dependence, and it was generally higher at 0.72 AU, perhaps owing to large data gaps in the PVO data set.

The solar-cycle dependence of the occurrence rate of Group 1 ICMEs agrees well with Richardson and Cane (2004), Huttunen *et al.* (2005), and Wu and Lepping (2007). In addition, we found as many as seven Group 1 ICMEs in 1987, in the rising phase of solar cycle 21, compatible with the unexpectedly large occurrence rate of MCs in 1997 found by Huttunen *et al.* (2005) as well as Wu, Lepping, and Gopalswamy (2006), because both 1987 and 1997 were in the rising phase. This suggests a higher possibility of seeing a relatively large amount of MCs a couple of years before solar maximum.

Overall, these results are consistent with the higher likelihood of a spacecraft penetrating the central flux rope (Group 1) at solar minimum. As noted in previous 1-AU studies (Jian *et al.*, 2006b), there are several factors causing a greater fraction of magnetic cloud signatures at solar minimum: weaker flux ropes affecting a smaller region in the ambient solar wind at solar minimum and also a simple (more dipolar) coronal structure at this time. These results could have different explanation if there are distinct classes of CMEs, one containing a MC and one not, or if MCs age or relax as they propagate from the Sun (Riley *et al.*, 2006).

A comparison between our preliminary 0.72-AU observations and the 1-AU observations has been given by Jian *et al.* (2008). The key results of this comparison incorporating the updated more complete statistics presented here are as follows.

From 0.72 to 1 AU, the SIR shock association rate increases significantly from 3% to 24%, consistent with Schwenn (1990), wherein, the ICME shock association rate changes more moderately, from 48% to 66%, compatible with the 50% of ICME shock association rate at 1 AU found by Marsden *et al.* (1987). The median duration of SIRs remains about 33 hours at both 0.72 and 1 AU, but their median width increases by 0.04 AU (0.20 to 0.24 AU), from Venus to Earth orbit. Since the mean velocity of SIRs only increases by 6% from 0.72 to 1 AU, the increase of the SIR width (product of mean velocity, duration, and $\sin\theta$) should be mainly due to the enhancement of the spiral angle.

In contrast, the ICMEs expand faster with their radial propagation, causing a larger increase of the width, by an amount of 0.1 AU. The radial variation of ICME width approximately follows $0.37R^{0.96}$ AU from 0.72 to 1 AU, consistent with the theoretical calibration by Chen (1996) and the *Helios* MC size variation $0.24R^{0.78}$ AU from 0.3 to 1 AU (Bothmer and Schwenn, 1998), except that our width includes sheath region if there is one. In contrast, the *Helios* ICME radius from Forsyth *et al.* (2006) has a variation $0.31R^{0.53}$ AU in the inner heliosphere, which indicates a smaller expansion than our result.

From Venus to Earth orbit, P_{tmax} of SIRs and ICMEs both decrease faster than the ambient solar wind, to about one-third their initial values. The B_{max} of ICMEs declines faster than the field in the ambient solar wind derived from the Parker (1958) solar-wind model, whereas the B_{max} of SIRs decreases slower than the field of the ambient solar wind. The B_{max} of ICMEs declines as about $16R^{-1.48}$ nT, similar to the radial variation of the mean B of ICMEs ($R^{-1.3}$ to $R^{-1.5}$) from Forsyth *et al.* (2006). The velocity enhancement across a SIR stays around 210 km s^{-1}. The ICME expansion speed remains around 110 km s^{-1} from 0.72 to 1 AU, in agreement with the nonsignificant radial dependence of ICME expansion speed found by Forsyth *et al.* (2006). This expansion speed is close to the Alfvén speed in the ICME.

We note that the two studies at 0.72 and 1 AU were conducted during different solar cycles, separated by one 22-year Hale cycle. If there is variation of the properties with solar cycle, the statistical radial comparison could be affected. However, in the future such solar-cycle-controlled differences should be able to be tested with inner heliosphere modeling efforts that can reproduce some of these basic observational trends from the observed

photospheric magnetic field patterns in the different solar cycles. In addition, the current *Venus Express* mission may be able to provide us with some solar-wind observations so that we can study the cycle-to-cycle variations in the future.

Acknowledgements This work has been jointly supported by the IGPP branch at Los Alamos National Lab (LANL) and by NASA's STEREO program through a grant administered by UCB. Work at Los Alamos was performed under the auspices of the U.S. Department of Energy. We thank the PIs of the instruments of the *Pioneer Venus Orbiter* mission for making the data available.

References

Aellig, M.R., Lazarus, A.J., Steinberg, J.T.: 2001, *Geophys. Res. Lett.* **28**, 2767.
Balogh, A., Gosling, J.T., Jokipii, J.R., Kallenbach, R., Kunow, H. (eds.): 1999a, *Space Sci. Rev.* **89**, 1.
Balogh, A., Bothmer, V., Crooker, N.U., Forsyth, R.J., Gloeckler, G., Hewish, A., *et al.*: 1999b, *Space Sci. Rev.* **89**, 141.
Belcher, J.W., Davis, L.: 1971, *J. Geophys. Res.* **76**, 3534.
Bothmer, V., Schwenn, R.: 1994, *Space Sci. Rev.* **70**, 215.
Bothmer, V., Schwenn, R.: 1998, *Ann. Geophys.* **16**, 1.
Burlaga, L.F.: 1974, *J. Geophys. Res.* **79**, 3717.
Burlaga, L.F.: 1991, In: Schwenn, R., Marsch, E. (eds.) *Physics of the Inner Heliosphere 2 – Particles, Waves and Turbulence*, Springer, Berlin, 1.
Burlaga, L.F., Sittler, E., Mariani, F., Schwenn, R.: 1981, *J. Geophys. Res.* **86**, 6673.
Cane, H.V., Richardson, I.G.: 2003, *J. Geophys. Res.* **108**(A4), SSH6-1.
Chen, J.: 1996, *J. Geophys. Res.* **101**, 27499.
Colin, L.: 1980, *J. Geophys. Res.* **85**, 7575.
Colin, L., Hunten, D.M.: 1977, *Space Sci. Rev.* **20**, 451.
Crooker, N.U.: 2000, *J. Atmos. Solar Terr. Phys.* **62**, 1071.
Feldman, W.C., Asbridge, J.R., Bame, S.J., Fenimore, E.E., Gosling, J.T.: 1981, *J. Geophys. Res.* **86**, 5408.
Forsyth, R.J., Bothmer, V., Cid, C., Crooker, N.U., Horbury, T.S., Kecskemety, K., *et al.*: 2006, *Space Sci. Rev.* **123**, 383.
Gopalswamy, N.: 2006, *J. Astrophys. Astron.* **27**, 243.
Gosling, J.T.: 1997, In: Crooker, N., Joselyn, J.A., Feynman, J. (eds.) *Coronal Mass Ejections, Geophys. Monograph* **99**, American Geophysical Union, 9.
Gosling, J.T., Forsyth, R.J.: 2001, *Space Sci. Rev.* **97**, 87.
Gosling, J.T., Pizzo, V.J.: 1999, *Space Sci. Rev.* **89**, 21.
Gosling, J.T., Asbridge, J.R., Bame, S.J., Feldman, W.C.: 1978, *J. Geophys. Res.* **83**, 1401.
Gosling, J.T., Borrini, G., Asbridge, J.R., Bame, S.J., Feldman, W.C., Hansen, R.F.: 1981, *J. Geophys. Res.* **86**, 5438.
Gosling, J.T., McComas, D.J., Phillips, J.L., Feldman, W.C.: 1991, *J. Geophys. Res.* **96**, 7831.
Hundhausen, A.J.: 1988, In: Pizzo, V.J., Holzer, T.E., Sime, D.G. (eds.) *Proceedings of the Sixth International Solar Wind Conference, Rep. NCAR/TN-306*, NCAR, Boulder, 181.
Huttunen, K.E.J., Schwenn, R., Bothmer, V., Koskinen, H.E.J.: 2005, *Ann. Geophys.* **23**, 625.
Intriligator, D.S., Siscoe, G.L.: 1994, *Geophys. Res. Lett.* **21**, 1117.
Intriligator, D.S., Wolfe, J.H., Mihalov, J.D.: 1980, *IEEE Trans. Geosci. Remote Sens.* **GE-18**, 39.
Jian, L.K., Russell, C.T., Gosling, J.T., Luhmann, J.G.: 2005a, In: Fleck, B., Zurbuchen, T.H., Lacoste, H. (eds.) *Proc. Solar Wind 11/SOHO 16 – Connecting Sun and Heliosphere, ESA SP-592*, 491.
Jian, L.K., Russell, C.T., Gosling, J.T., Luhmann, J.G.: 2005b, In: Fleck, B., Zurbuchen, T.H., Lacoste, H. (eds.) *Proc. Solar Wind 11/SOHO 16 – Connecting Sun and Heliosphere, ESA SP-592*, 731.
Jian, L.K., Russell, C.T., Luhmann, J.G., Skoug, R.M.: 2006a, *Solar Phys.* **239**, 337.
Jian, L.K., Russell, C.T., Luhmann, J.G., Skoug, R.M.: 2006b, *Solar Phys.* **239**, 393.
Jian, L.K., Russell, C.T., Luhmann, J.G., Skoug, R.M.: 2008, *Adv. Space Res.* **41**, 259.
Klein, L.W., Burlaga, L.F.: 1982, *J. Geophys. Res.* **87**, 613.
Krieger, A.S., Timothy, A.F., Roelof, E.C.: 1973, *Solar Phys.* **29**, 505.
Lepping, R.P., Jones, J.A., Burlaga, L.F.: 1990, *J. Geophys. Res.* **95**, 11957.
Lindsay, G.M., Russell, C.T., Luhumann, J.G., Gazis, P.: 1994, *J. Geophys. Res.* **99**, 11.
Luhmann, J.G.: 1986, *Space Sci. Rev.* **44**, 241.
Luhmann, J.G., Cravens, T.E.: 1991, *Space Sci. Rev.* **55**, 201.
Luhmann, J.G., Kasprzak, W.T., Russell, C.T.: 2007, *J. Geophys. Res.* **112**, E04S10.

Luhmann, J.G., Li, Y., Arge, C.N., Gazis, P., Ulrich, R.: 2002, *J. Geophys. Res.*, 107.
Mariani, F., Neubauer, F.M.: 1990, In: Schwenn, R., Marsch, E. (eds.) *Physics of the Inner Heliosphere 1 – Large-Scale Phenomena*, 183.
Marsden, R.G., Sanderson, T.R., Tranquille, C., Wenzel, K.-P., Smith, E.J.: 1987, *J. Geophys. Res.* **92**, 11009.
Marubashi, K.: 1997, In: Crooker, N., Joselyn, J.A., Feynman, J. (eds.) *Coronal Mass Ejections, Geophys. Monograph* **99**, American Geophysical Union, 147.
Mulligan, T., Russell, C.T., Luhmann, J.G.: 1998, *Geophys. Res. Lett.* **25**, 2959.
Neugebauer, M., Goldstein, R.: 1997, In: Crooker, N., Joselyn, J.A., Feynman, J. (eds.), *Coronal Mass Ejections*, *Geophys. Monograph* **99**, American Geophysical Union, 245.
Neugebauer, M., Liewer, P.C., Goldstein, B.E., Zhou, X., Steinberg, J.T.: 2004, *J. Geophys. Res.*, 109.
Osherovich, V., Burlaga, L.F.: 1997, In: Crooker, N., Joselyn, J.A., Feynman, J. (eds.) *Coronal Mass Ejections*, *Geophys. Monograph* **99**, American Geophysical Union, 157.
Parker, E.N.: 1958, *Astrophys. J.* **128**, 664.
Pilipp, W.G., Miggenrieder, H., Muhlhauser, K.-H., Rosenbauer, H., Schwenn, R.: 1990, *J. Geophys. Res.* **95**, 6305.
Pizzo, V.J.: 1978, *J. Geophys. Res.* **83**, 5563.
Plunkett, S.P., Vourlidas, A., Šimberová, S., Karlický, M., Kotrč, P., Heinzel, P., Kupryakov, Yu.A., Guo, W.P., Wu, S.T.: 2000, *Solar Phys.* **194**, 371.
Richardson, I.G., Cane, H.V.: 2004, *Geophys. Res. Lett.* **31**, L18804.
Richardson, I.G., Cliver, E.W., Cane, H.V.: 2000, *J. Geophys. Res.* **105**(A8), 18203.
Richter, A.K., Luttrell, A.H.: 1986, *J. Geophys. Res.* **91**(A5), 5873.
Riley, P., Schatzman, C., Cane, H.V., Richardson, I.G., Gopalswamy, N.: 2006, *Astrophys. J.* **647**, 648.
Russell, C.T.: 1991, *Space Sci. Rev.* **55**, 1.
Russell, C.T., Shinde, A.A.: 2005, *Solar Phys.* **229**, 323.
Russell, C.T., Vaisberg, O.L.: 1983, In: Hunten, D.M., Colin, L., Donahue, T.M., Moroz, V.I. (eds.) *Venus*, University of Arizona Press, Tuscon, 873.
Russell, C.T., Shinde, A.A., Jian, L.K.: 2005, *Adv. Space Res.* **35**, 2178.
Russell, C.T., Snare, R.C., Means, J.D., Elphic, R.C.: 1980, *IEEE Trans. Geosci. Remote Sens.* **GE-18**, 32.
Rust, D.M., Anderson, B.J., Andrews, M.D., Acuña, M.H., Russell, C.T., Schunk, P.W., Mulligan, T.: 2005, *Astrophys. J.* **621**, 524.
Schwenn, R.: 1990, In: Schwenn, R., Marsch, E. (eds.) *Physics of the Inner Heliosphere 1 – Large-Scale Phenomena*, Springer, Berlin, 99.
Schwenn, R., Marsch, E. (eds.): 1990, *Physics of the Inner Heliosphere 1 – Large-Scale Phenomena*, Springer, Berlin.
Sheeley, N.R. Jr., Howard, R.A., Koomen, M.J., Michels, D.J., Schwenn, R., Mühlhäuser, K.H., Rosenbauer, H.: 1985, *J. Geophys. Res.* **90**, 163.
Smith, E.J., Wolfe, J.H.: 1976, *J. Geophys. Res.* **3**, 137.
Song, W., Wang, J.: 2006, *Astrophys. J.* **643**, 69.
Suess, S.T., Hildner, E.: 1985, *J. Geophys. Res.* **90**, 9461.
Vaisberg, O.L., Zeleny, L.M.: 1984, *Icarus* **58**, 412.
Wang, C., Du, D., Richardson, J.D.: 2005, *J. Geophys. Res.* **110**, A10107.
Wimmer-Schweingruber, R.F., Crooker, N.U., Balogh, A., Bothmer, V., Forsyth, R.J., Gazis, P., *et al.*: 2006, *Space Sci. Rev.* **123**, 177.
Wu, C.C., Lepping, R.P.: 2007, *Solar Phys.* **242**, 159.
Wu, C.C., Lepping, R.P., Gopalswamy, N.: 2006, *Solar Phys.* **239**, 449.
Zurbuchen, T.H., Richardson, I.G.: 2006, *Space Sci. Rev.* **123**, 31.